THESIS FOR THE DEGREE OF LICENTIATE OF ENGINEERING

Developments Toward a Novel Methodology for Spent Nuclear Fuel Verification

Moad S. Al-dbissi

Department of Physics
Chalmers University of Technology
Gothenburg, Sweden 2022

Developments Toward a Novel Methodology for Spent Nuclear Fuel Verification.

Moad S. Al-dbissi

Division of Subatomic, High Energy and Plasma Physics
Department of Physics
Chalmers University of Technology
SE-412 96 Gothenburg
Sweden
Telephone +46(0)31-772 1000

Cover:
Vertical and horizontal cross section view of the gradient detector concept.

Chalmers Digital Print
Gothenburg, Sweden 2022

Developments Toward a Novel Methodology for Spent Nuclear Fuel Verification

Moad Al-dbissi
Division of Subatomic, High Energy and Plasma Physics
Department of Physics
Chalmers University of Technology

Abstract

One of the tasks in nuclear safeguards is to regularly inspect spent nuclear fuel discharged from nuclear power reactors and verify the integrity of it, so that illegal removal and diversion of radioactive material can be promptly discovered. In the current project, which is a collaboration between Chalmers University of Technology and SCK CEN, a novel methodology for non-intrusive inspection of spent nuclear fuel is under development. The methodology consists of two main steps: 1) neutron flux and its gradient are measured inside spent nuclear fuel assemblies using small neutron detectors; and 2) the measurements are processed using an Artificial Neural Network (ANN) algorithm to identify the number and location of possible fuel pins that have been removed from the fuel assemblies and/or replaced with dummies. The use of small neutron detectors simplifies the inspection procedure since the fuel assemblies are not moved from their storage position. In addition, the neutron flux gradient measurements and its processing with the ANN algorithm have the potential for more detailed results. Different aspects have been investigated for the development of the methodology. For the first step of the methodology, the concept of a new neutron detector has been studied via Monte Carlo simulations and it relies on the use of optical fiber-mounted neutron scintillators. The outcome of the computational study shows that the selected detector design is a viable option since it has a suitable size to be introduced inside a fuel assembly and can measure neutron flux gradients. Then, experimental work has been carried out to test and characterize two optical fiber-based neutron scintillators that can be used to build the detector, with respect to detection of thermal neutrons and sensitivity to gamma radiation. For the second step of the methodology, a machine learning algorithm based on ANN is studied. At this initial stage, a simpler problem has been considered, i.e., an ANN has been prepared, trained and tested using a dataset of synthetic neutron flux measurements for the classification of PWR nuclear fuel assemblies according to the total amount of missing fuel, without including neutron flux gradient measurements and without localizing the anomalies. From the comparison with other machine learning methods such as decision trees and k-nearest neighbors, the ANN shows promising performance.

KEYWORDS: nuclear safeguards, spent nuclear fuel, partial defect, neutron scintillator, flux gradient detector, machine learning, artificial neural networks

List of Publications

Paper I

Aldbissi, M., Vinai, P., Borella, A., Rossa, R., Pázsit, I. (2022). Conceptual design and initial evaluation of a neutron flux gradient detector. Nuclear Instruments and Methods in Physics Research Section A: Accelerators, Spectrometers, Detectors and Associated Equipment, 1026, 166030. https://doi.org/10.1016/j.nima.2021.166030

Paper II

Aldbissi, M., Vinai, P., Pázsit, I., Borella, A. Rossa, R. (2021). Conceptual design and initial evaluation of a neutron flux gradient detector for partial defect testing of spent nuclear fuel. INMM/ESARDA Joint Annual meeting, August 2021. https://resources.inmm.org/annual-meeting-proceedings/conceptual-design-and-initial-evaluation-neutron-flux-gradient-detector

The author's contribution to the included papers

Paper I and Paper II: Aldbissi, M. developed all the Monte-Carlo models, performed all the simulation work, and generated the plots and the tables included in the paper. The development of the theoretical concepts, the interpretation of the results, and the writing of the papers was done in collaboration with the co-authors.

Acknowledgments

I would like to thank my supervisors Assoc. Prof. Paolo Vinai and Prof. Imre Pazsit at Chalmers University of Technology, and Dr. Alessandro Borella and Dr. Riccardo Rossa at The Belgian Nuclear Research Centre (SCK CEN), for all their guidance and support and for all their contributions to the project.

The experimental work at Chalmers University of Technology was made possible by the help and effort of Anders Nordlund, Lennart Norberg and Lasse Urholm, and at SCK CEN by the help of Eric Boogers, Luc Borms and Bart Van Houdt.

The computational work was enabled by resources provided by the Swedish National Infrastructure for Computing (SNIC) at the Chalmers Centre for Computational Science and Engineering (C3SE), and at the National Supercomputer Centre (NSC), Linköping University (LiU), partially funded by the Swedish Research Council through grant agreement no. 2018-05973.

The project was also financially supported by SCK CEN under grant agreement PO4500047684, the Swedish Radiation Safety Authority under agreement SSM2021-709-19, the Ringhals power plant and from the Euratom research and training programme 2014-2018 under grant agreement No 847594 (ARIEL).

We are grateful to Prof. T. Misawa, Prof. Y. Kitamura and Dr. Y. Takahashi, Institute for Integrated Radiation and Nuclear Science, Kyoto University (KURNS), for providing us two optical fiber-based neutron scintillators.

I would also like to thank my family for their continuous love, support and encouragement throughout the years of my studies.

Contents

List of Figures

List of Tables

1 Introduction

In this chapter the area of research is introduced in section 1.1 , the objectives of the project are discussed in section 1.2, and the structure of the thesis is provided in section 1.3.

1.1 Background

Nuclear energy is an energy source that may contribute to the energy mix needed for a more sustainable society because of its small carbon footprints and by serving as a reliable base-load. It is currently used in over 30 countries producing approximately 10% of global electricity from about 440 nuclear power plants [1].

The complexity of nuclear technology and the harmful consequences that can result if this technology is misused are undeniable. In order to assure that Non-Nuclear Weapon States (NNWS) honor their international obligations and in order to detect any diversion of nuclear material or technology promptly, a set of technical measures referred to as safeguards [2] must be applied in all nuclear facilities.

One of the most important tasks in nuclear safeguards that must be carried out in any nuclear power plant is regular inspections to verify that no special nuclear material is missing from the spent nuclear fuel assemblies. In the safeguards community, such a task is known as detection of partial defects [3]. These assemblies are discharged from the reactor core at the end of their life and are highly radioactive. They are temporarily stored in a water pool before they are sent to either a dry storage facility, a final underground repository or a reprocessing facility. Spent nuclear fuel is particularly sensitive from a safeguards perspective because of its residual fissile material such as uranium-235 and plutonium-239. In the recent years, about 80% of the material placed under safeguards was plutonium contained in spent fuel [4].

Currently, several methods of Non-Destructive Assay (NDA) such as the Digital Cherenkov Viewing Device (DCVD), the Passive Gamma Emission Tomography (PGET) and the Fork Detector (FD) among others are used to detect possible diversions in spent fuel assemblies. These techniques are verified by the International Atomic Energy Agency (IAEA) and have been extensively applied for many years, but they also have limitations.

The DCVD is based on the measurement of the Cherenkov (ultraviolet) light produced by the gamma radiation escaping the fuel assembly and interacting with water. The method is limited to wet storage and the interpretation of the Cherenkov images is not algorithmic, rather it requires a subjective decision from the inspector [5].

The PGET is based on the measurement of the two-dimensional intensity distribution of gamma radiation emitted mainly by Cesium-137. The method has a good identification accuracy up to one-rod level [6] but it requires long measurement times ($\sim$ hours) and the movement of the fuel assemblies from their original storage position [5].

The FD uses a combination of gas-filled fission chambers and gas-filled ionization chambers to detect both neutrons and gamma particles, respectively. The method has a high level of maturity with a long history of applications. However, it also requires the movement of the fuel from its original storage position [5]. Previous studies suggest that specific diversion configurations can be designed in which the fork detector will not notice a difference between an intact assembly

and an assembly with up to 50% missing fuel pins especially if the diversions are in the central region of the assembly [7].

1.2 Objectives of the project

In an attempt to enhance safeguards inspections of spent fuel, the current research aims at developing a methodology that can be accurate and non-intrusive and that does not require the movement of the assemblies. The strategy of the methodology is to measure the neutron flux and its gradient within a spent fuel assembly, and to identify possible anomalies and their locations from an algorithmic processing of such information.

For the measurement of the neutron flux and its gradient inside the spent fuel assembly, a small neutron detector that can be inserted in the system and can detect simultaneously neutrons at multiple locations (and thus be angularly sensitive) is needed. Such a detector can be constructed as a cluster of thin light guiding fibers on whose tips a small volume of a mixture of neutron converter and scintillation material is mounted.

These types of optical fiber-based neutron scintillators were first developed and successfully tested in Japan [8, 9, 10]. Efforts have been made in further development and characterization at EPFL, e.g., see [11]. Recent work has also shown the suitability of using a cluster of optical fiber-based scintillators for high-resolution neutron flux measurements and for the characterization of highly localized gradients [12].

The identification of missing fuel pins from measurements is a so-called "inverse task", i.e., the unknown system configuration (the arrangement of fuel pins) is determined from measurable, observable quantities (the neutron flux and its gradient), which originated from the system configuration itself. In the current context, a machine learning algorithm based on an Artificial Neural Network (ANNs) is investigated for the inversion problem.

Recent research has shown the potential of machine learning for different inverse tasks in nuclear technology [13], e.g.: the identification and localization of perturbations in nuclear reactor cores from neutron flux measurements [14, 15, 16]; the prediction of Pressurized Water Reactor (PWR) spent fuel parameters from observable quantities such as gamma, neutron and Cherenkov intensities [17]; the detection and localization of missing radioactive sources within a small grid [18]; data analysis in tracking elemental and isotopic material flows through material balance areas for safeguards [19]; and the detection of missing fuel pins in PWR spent fuel assemblies [20, 21].

1.3 Structure of the thesis

The thesis is built from the content of Paper I and Paper II and includes additional content that has not been published yet. The structure is as follows. Chapter 2 summarizes Paper I and Paper II and mainly concerns the conceptual design and initial evaluation of a gradient detector suitable for the methodology under development. Chapter 3 describes the experimental work that was performed at Chalmers and at SCK CEN for the characterization of two optical fiber-based neutron scintillators. Chapter 4 discusses the initial development and training of an ANN for the methodology. Chapter 5 provides conclusions and an outlook for the continuation of the work.

2 Conceptual study of the neutron flux gradient detector

The conceptual design of a flux gradient detector, suitable for the planned measurements within the fuel assembly, as one phase of the full project, is investigated. First, the design of the detector is described in section 2.1. Then, a model for the Monte Carlo simulation of the detector behavior and a test case for the evaluation of the detector performance are introduced in section 2.2. Finally, the results of the simulations are discussed in section 2.3.

2.1 Detector design

As mentioned earlier, a detector can be constructed from several small optical fiber-based neutron detectors [12], to measure concurrently the scalar flux in several positions over a two-dimensional plane and thus determine the scalar flux gradient. The diameter of the individual fiber-based detectors can be as small as about one mm, however, the diameter of the gradient detector will be inevitably larger. By aiming at performing measurements within a nuclear fuel assembly, one can use the instrumentation guide tubes of the assembly, which are about 1 cm in diameter.

A gradient detector, capable of measuring the two components of the flux gradient in the x-y plane, with the mentioned size limitation, is proposed as follows. An aluminum cylinder of a diameter of 1 cm with four axial holes arranged in a rectangular pattern serve as holder of four fiber-mounted scintillation detectors, as shown in Figure 2.1. Each of the fibers is inserted into one of the holes from above, and its tip is covered in the neutron sensitive converter and scintillation material, as shown in Figure 2.1. Aluminum is chosen for the cylinder because of its easy manufacturing properties, and low neutron absorption cross section.

The complete detector containing four fibers can be inserted into the instrumentation guide tube and moved to a suitable axial position. Then the two detector pairs at diagonally opposite positions, perpendicular to each other, can be used to measure the two horizontal components of the flux gradient.

2.2 Monte-Carlo model

Whereas it is intuitively clear that, in theory, the detector design described earlier is suitable to determine the flux gradient, it is useful to assess its performance by detailed simulations. For this purpose, the open-source code Serpent is used [22]. Serpent is a multi-purpose three-dimensional continuous-energy Monte Carlo particle transport code developed at VTT, the Technical Research Centre of Finland. The code is designed for traditional reactor physics applications, for multi-physics reactor calculations, and for neutron and photon transport calculations in radiation, fusion and medical physics problems. Serpent also includes numerical capabilities that allow parallel computing on clusters and multi-core workstations.

The Serpent model of the gradient detector is shown in Figure 2.2. There exist several different options for small size neutron detectors in terms of neutron converter and scintillation material (LiCaF, boron loaded plastic scintillator, etc.). We restrict the present study to the type of detectors which we have at hands and which were also used in previous works [11], namely LiF as neutron converter and ZnS(Ag) as the scintillation material.

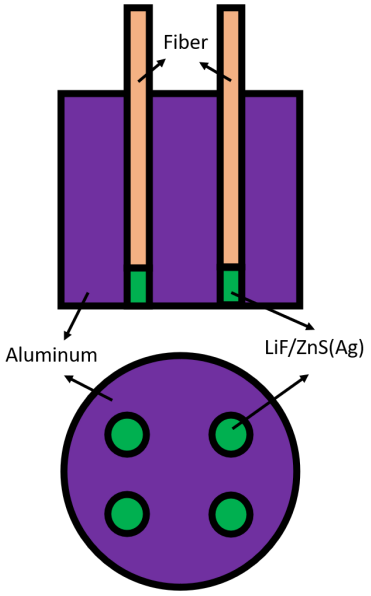

Figure 2.1: Vertical and horizontal cross section view of the detector concept.

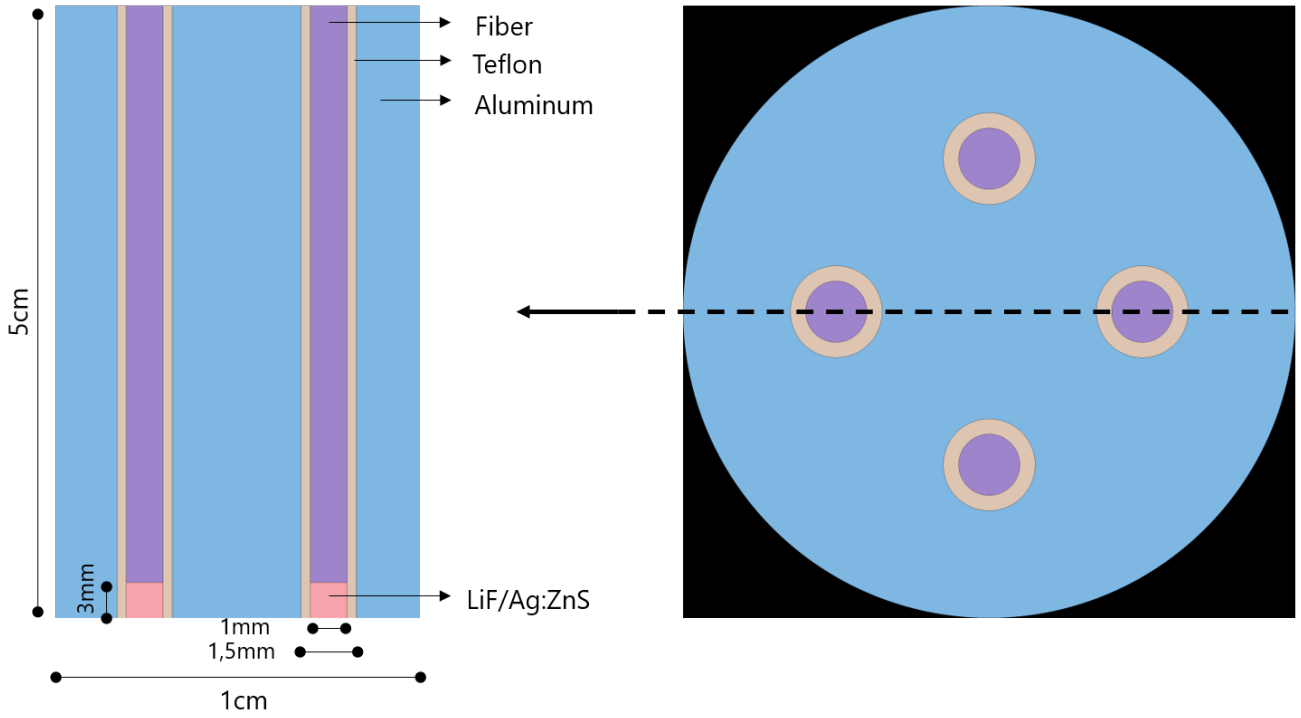

Figure 2.2: LiF-based gradient detector as modelled in Serpent.

To assess the performance of the detector, a hypothetical test case is considered. The test case was chosen to be similar to that used in earlier works, i.e., a neutron source in a water tank [23, 24]. The reason is partly that it is a simple setup, with an azimuthally symmetric flux distribution in the horizontal plane, in which the results can be easily interpreted. And partly, because such an experiment will be possible to carry out at a later stage of the project, when the detector will actually be fabricated. The general layout is shown in Figure 2.3. It consists

of a cylindrical Aluminum tank 1m in height and 1m in diameter filled with water, with a ^{252}Cf source, 2 cm in diameter, in the middle.

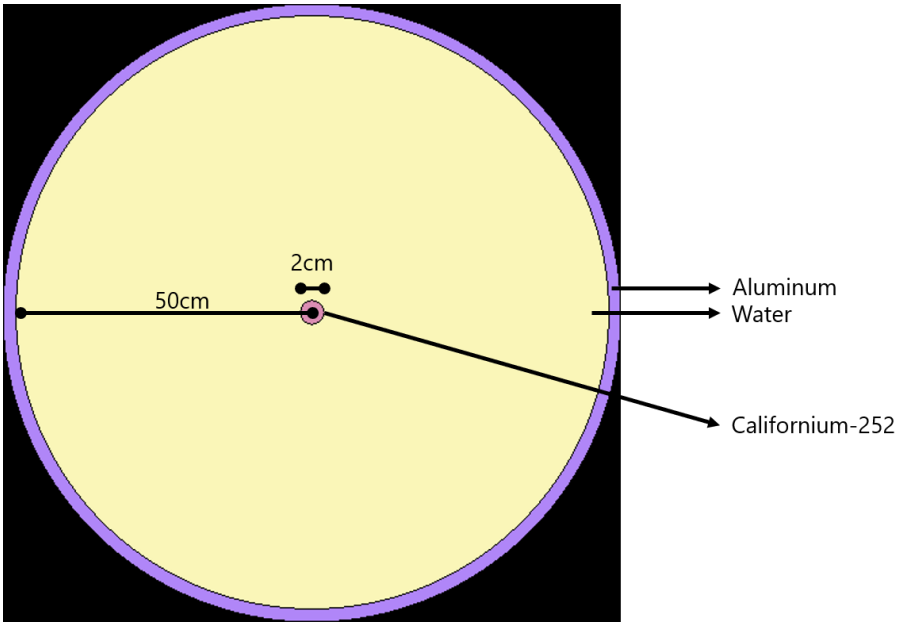

Figure 2.3: Setup used for the evaluation of the detector, as modelled in Serpent.

The motivations behind the Monte Carlo simulations of the detector behavior are twofold. First, similarly to the case of the ordinary neutron detectors, the presence of the detector might interfere with the neutron flux distribution. The consequences of such a flux disturbance are usually not significant when measuring the scalar flux. However, the detector under study will give an estimation of the gradient from the difference between the neutron flux values that are measured by the four scintillators, which are placed relatively close to each others. The potential distortion introduced with the four scintillators might have a more substantial impact on the determination of the flux gradient than on the scalar flux. Second, a systematic underestimation of the gradient might arise from a self-shielding effect, i.e., the scintillators at the higher flux position might shield against the neutron current pointing to the scintillators at the lower flux position. Then it is important to investigate quantitatively these effects and to understand whether they are relevant and need to be compensated by some procedures or not.

2.3 Simulations and analysis

The simulations performed in this work are restricted to the neutronic aspects of the measurement, i.e. calculating the reaction rates in the detector. The generation and transport of the scintillation light are not taken into consideration, since they would require a substantially larger effort, with a rather modest extra information.

The performance of the detector to determine the magnitude (section 2.3.1) and the direction (section 2.3.2) of the neutron flux gradient is investigated via Monte Carlo calculations in the hypothetical measurement setup described in section 2.2. Different positions and orientations of the detector in the water tank, and the effect of the different efficiency of the scintillators, e.g. due to non-identical ^{6}Li content, were considered (section 2.3.3).

2.3.1 Magnitude of the gradient

As mentioned in Section 2.2, one goal is to investigate how the presence of the detector affects the accuracy of the estimation of the gradient. The strategy to quantify this effect relies on two sets of simulations. The first simulation does not include the detector and the "unperturbed" thermal neutron flux is calculated in hypothetical measurement positions where the gradient detector can be inserted. In the second step, simulations are made for the case that the detector occupies the positions previously selected, one at a time, and the reaction rates in the scintillators are calculated. The gradient obtained from the difference of the reaction rates of the diagonally opposite scintillator pairs is then compared with the gradient of the neutron flux obtained without the detector.

The comparison between the gradient from the unperturbed flux and the gradient from the reaction rates is not completely trivial. At any single measurement point, the magnitude of the gradient will be quantitatively different for the flux and the reaction rate, since they correspond to physically different quantities. Nevertheless, the two are proportional to a scaling factor which can be considered as a constant for a given energy distribution. The scaling factor does not depend on the actual value of the gradient, and hence on the measurement position. If the space dependence of the two gradients is proportional to a constant scaling factor, then it is a demonstration of the equivalence between the two gradients and the negligible effect of the presence of the detector.

In the simulations with the detector, the detector orientation is chosen such that two scintillators are lined up on the x-axis, i.e. the line connecting two of the scintillators points to the source (towards the centre of the water tank). Because of the azimuthal symmetry of the setup, these two scintillators measure the radial component of the gradient (i.e. its x-component), whereas the azimuthal component of the flux gradient is zero. Hence, the radial component is equal to the x-component of the gradient. This can be characterised by the signed magnitude of the gradient, i.e. a positive value when the gradient is pointing outwards from the centre, and negative when the gradient points towards the centre. The Serpent model of this arrangement is shown in Figure 2.4.

The signed magnitude of the neutron flux gradient without the detector and that obtained from the reaction rates estimated in the scintillators of the detector are compared at different distances from the neutron source, see Figure 2.5. The two curves are normalized to each other using the least square fit method. The space dependence of the two gradients are very close, indicating that the distortion effect of the proposed detector design is negligible.

2.3.2 Direction of the gradient vector

The two-dimensional flux gradient has two Cartesian components which carry independent information. Instead of using these two components, the space dependence of the magnitude (absolute value) and of the direction of the gradient are used because they are more effective features in a pattern recognition or any other identification/unfolding task and because their physical meaning is easier to interpret.

Therefore, the suitability of the detector to estimate the direction of the gradient vector is investigated. A general case with non-zero components of the gradient is considered, i.e., the

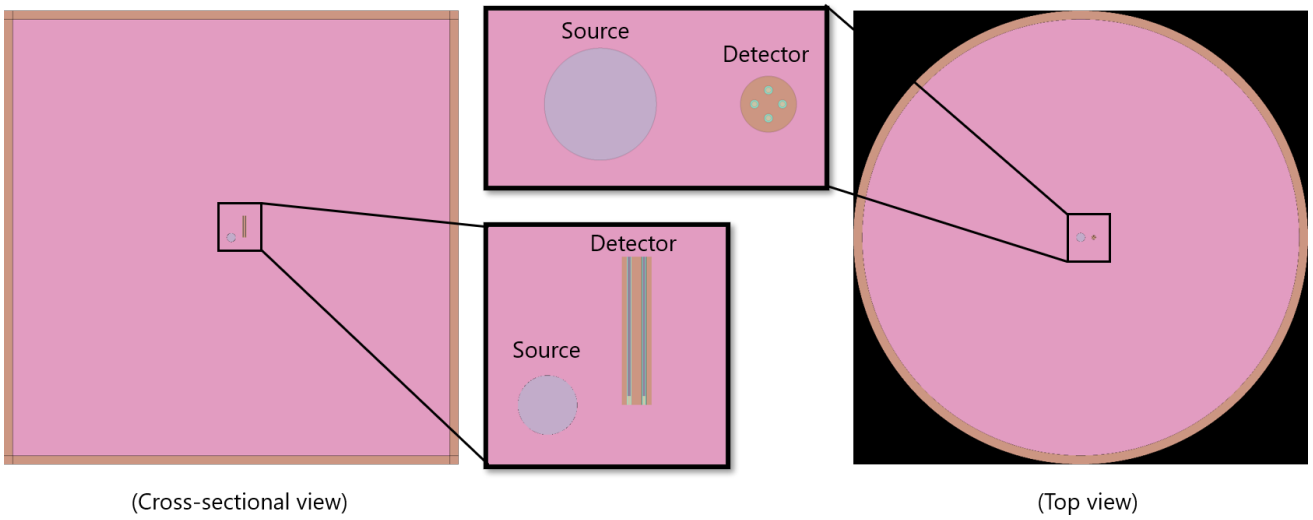

Figure 2.4: The Serpent model for the simulation of the measurement of the radial component of the gradient.

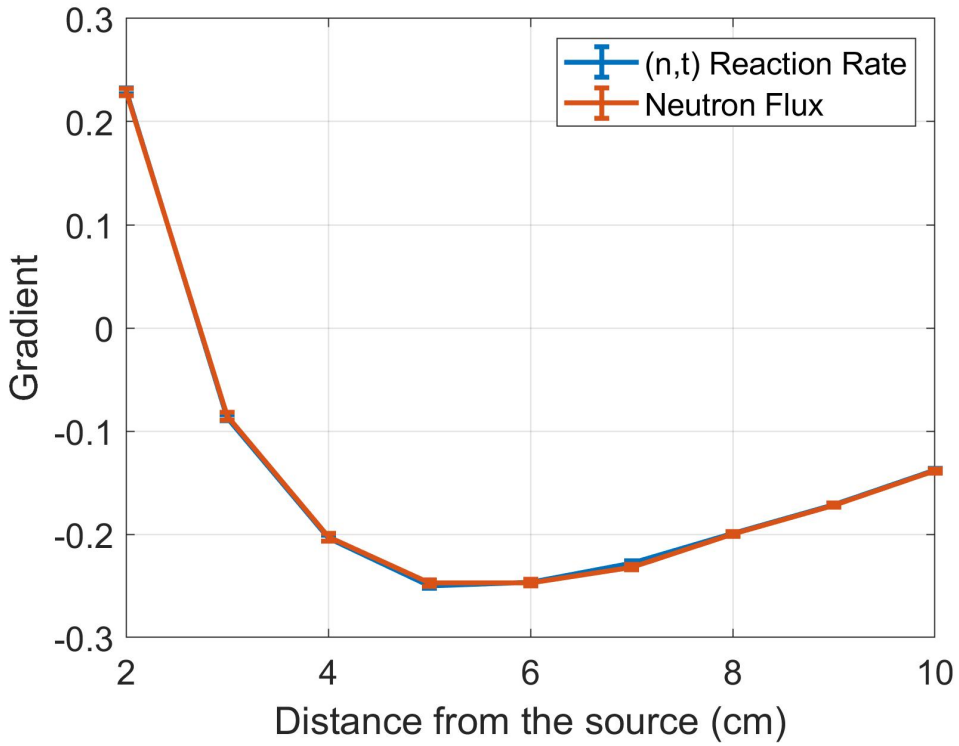

Figure 2.5: The normalized spatial dependence of the radial component of the gradient with and without the presence of the detector.

detector is positioned such that none of the two scintillator pairs lie on a radial line from the neutron source. Other special orientations are also avoided, e.g., when the angle between the two scintillator lines and the x axis is $\pm 45°$. The system configuration is then chosen where the detector is rotated 30° counterclockwise as compared to the calculations in the previous

Subsection. An illustration of this case is given in Figure 2.6. Several simulations were performed with the detector at different positions along the x axis. The results from the calculated reaction rates show, also through a comparison with Figure 2.5, that the direction angle of the gradient is estimated correctly, see Figure 2.7. One advantage of the direction of the gradient is that it does not require any normalisation, i.e., it can be directly compared to the expected (true) value of the direction.

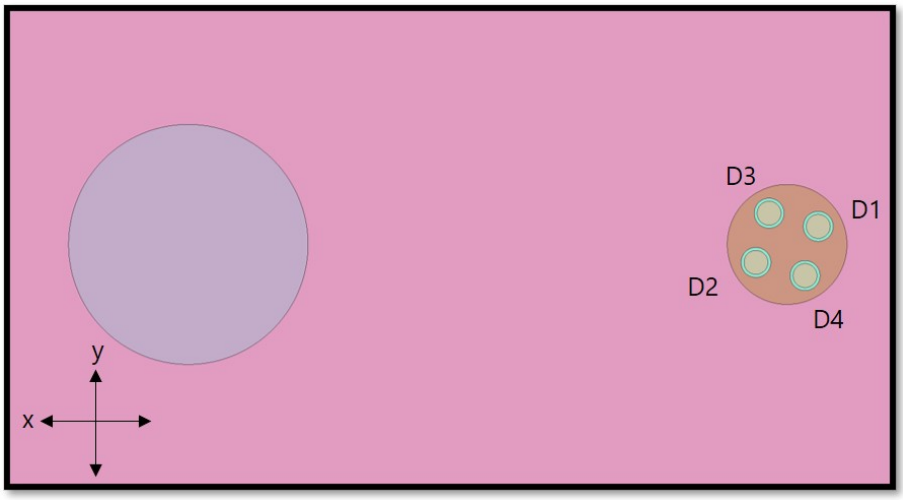

Figure 2.6: Serpent model for the measurement of the direction of the gradient with the detector shifted in a 30° angle counterclockwise.

2.3.3 Effect of the differences in the scintillators

In the simulations so far, it was assumed that all four scintillators are equal and thus have the same efficiency. A quantitative investigation of the effect of different sensitivities of the scintillators, and the methods for correcting them, are also of interest.

Scintillators manufactured at an industrial level can be bought. However, as a rule, these are of larger size (thicker) than what is necessary for the current application. Hence, the prototype of the detector which will be built in this project will be based on thin LiF-ZnS(Ag) scintillators, whose manufacturing follows an artisanal process, which may impact the uniformity and precision of the instrument. Therefore, the four scintillators may slightly differ from each other in terms of the amount of neutron converter and scintillation material. Even if the scintillators can be calibrated in laboratory measurements separately (see section 3.3), their efficiencies may not be the same in the device because of the mounting material, the surrounding matrix, the optical coupling of the fiber to both the scintillator and the Photo-Multiplier (PM) tube needed for the generation of the signal for the data acquisition system (see section 3.1). Therefore, after the scintillators are mounted in the detector, their individual efficiencies become more complicated to determine.

On the other hand, one does not need the absolute efficiencies of the four scintillators, only the efficiencies relative to each other, and a method to compensate for them. As mentioned earlier, the flux gradient is only determined to a constant scaling factor, whose value is not of interest. However, since scintillators with different efficiencies do not measure the same neutron flux values at a specific position, changes in the orientation of the scintillators might affect the scaling

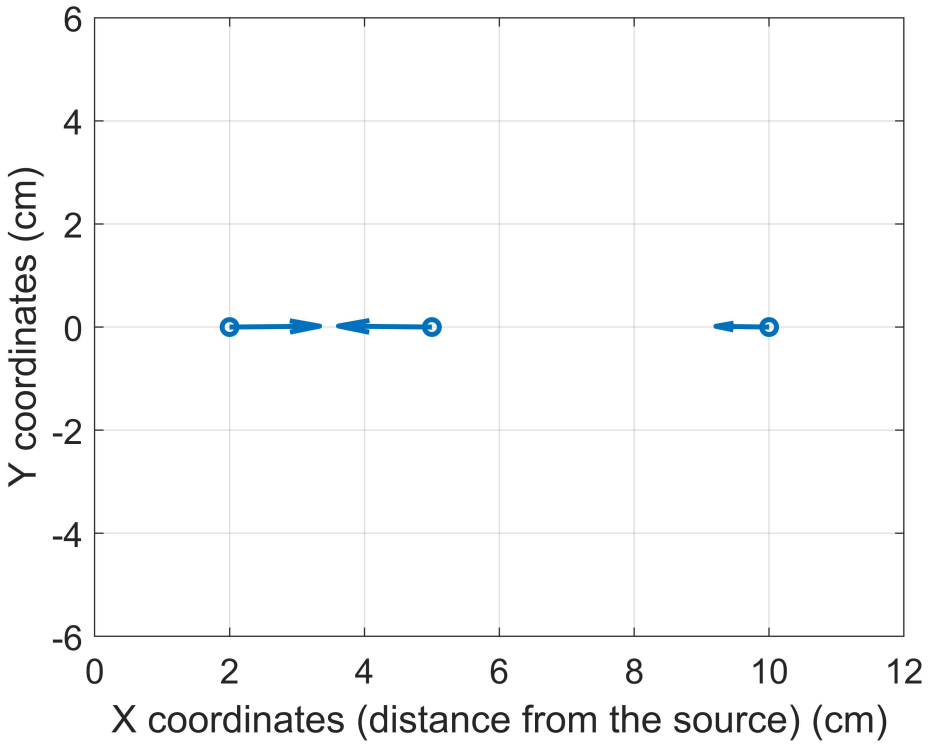

Figure 2.7: Estimated direction of the gradient vector at different locations of the detector along the x-axis.

factor. The purpose of the correction is thus to make sure that a constant scaling is preserved, irrespective of the orientation of the detector. Such correction methods are quantitatively investigated in Paper II. The correction method used in the current study amounts to an in-situ calibration of the relative efficiencies, which can be even performed in a field measurement, and has to be executed only once.

In the case of a detector with four scintillators of varying efficiencies, the correction method is based on rotating the detector by 90°, 180° and 270° from its original orientation. Accordingly, each scintillator occupies the four angular positions once, providing four reaction rates that allow to calculate an average value. Then the two components of the gradient are determined by taking the difference of the average reaction rates of the diagonally opposing scintillators. Such a correction method will lead to an unbiased estimate of the gradient and to the relative efficiencies of the four scintillators. The relative efficiencies can be used to correct the measurements in other points, without the need for additional rotations of the detector.

In order to investigate the effect of having imperfect scintillators on the estimation of the flux gradient, 4 scenarios are considered. In the first scenario, one of the four scintillators is altered to have a lower atomic fraction of ^{6}Li and hence a lower efficiency. The second scenario is such that the detector defined in the first scenario is tested with a different orientation. In the third scenario, the gradient detector consists of 4 scintillators, each with a different content of ^{6}Li. In the fourth scenario, the detector with 4 different scintillators is studied adding a possible uncertainty to the initial position and the rotation angles. The results for these scenarios are

discussed in details in Paper II.

An illustrative example of these results is shown in Figure 2.8, where the fourth scenario (represented by the yellow arrow) is compared with the ideal scenario (blue arrow), given a fixed position of the detector with respect to the neutron source. In the ideal scenario, the four scintillators have the exact same material composition and the detector is placed accurately at 30° as its initial orientation. In the fourth scenario, the atomic fractions of ^{6}Li is 100% for D1, 80% for D2, 70% for D3, and 60% for D4, and the detector is rotated with 92° (instead of 90°), 179° (instead of 180°), and 273° (instead of 270°) during the calibration. For the comparison, an additional scenario (red arrow) is considered, in which the four scintillators have the same material composition but an error is assigned to the ideal orientation angle, i.e., the detector is shifted of 27° with respect to the x-axis. Both the magnitude and the direction of the gradient vector can be reconstructed despite the varying efficiencies of the scintillators and the uncertainty in the initial positioning of the detector or in the rotation angles during the calibration process.

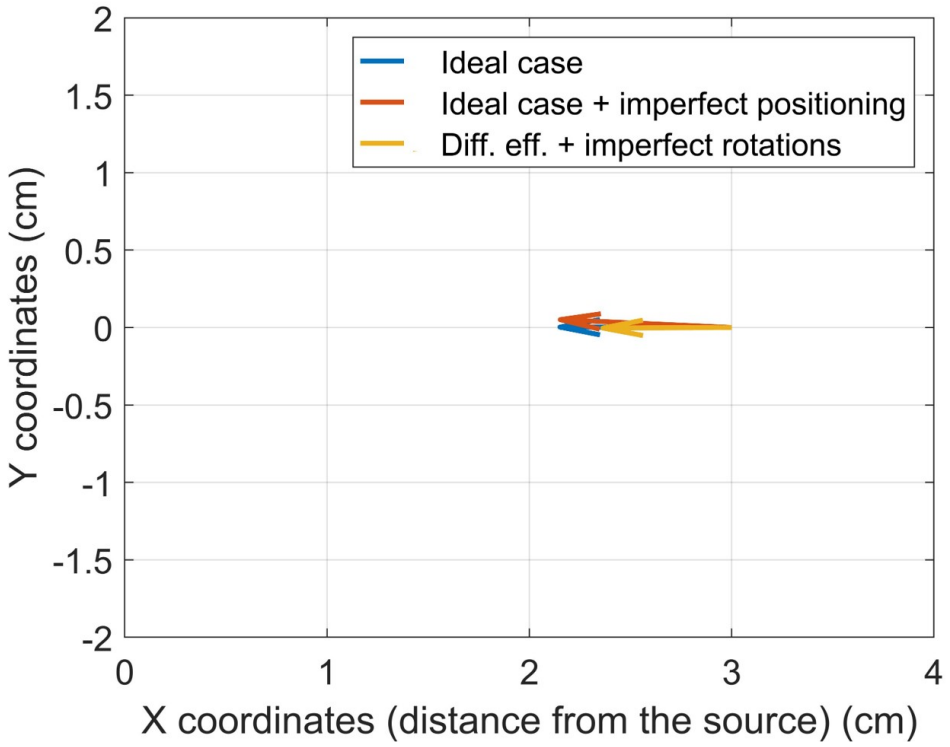

Figure 2.8: Estimated direction of the flux gradient with imperfect efficiencies, positions and rotations during the calibration

3 Characterization of optical fiber-based neutron scintillators via experiments

Two optical fiber-based neutron scintillators, on which the concept of the gradient detector described in the previous chapter is based, were tested and characterized. The two scintillators are of the same type and are briefly described in section 3.1. The sensitivity of the two scintillators to thermal neutrons was tested in the presence of a neutron source in the hot-cell laboratory at the Department of Physics, Chalmers University of Technology, see section 3.2. Further testing was carried out in the BR1 research reactor at SCK CEN, where the two scintillators were exposed to a well-known Maxwellian thermal flux, see section 3.3. The sensitivity to gamma rays was investigated using calibrated gamma sources with various strengths in the Laboratory for Nuclear Calibration (LNK) at SCK CEN, see section 3.4.

3.1 Optical fiber-based scintillators

Two optical fiber-based neutron scintillators of the same type are available in the current project, courtesy of Kyoto University Institute for Integrated Radiation and Nuclear Science (KURNS), Japan. Their testing and characterization is useful for the future construction of the gradient detector discussed in the previous chapter.

Each of them consists of a ~ 2 m long and ~ 1 mm thin plastic optical fiber whose tip is covered with a LiF-ZnS(Ag) material as shown in Figure 3.1. The tip of the fiber acts as the neutron sensitive part, where LiF is the neutron converter according to the reaction [11]

$$^{6}\mathrm{Li} + \mathrm{n} \longrightarrow {}^{4}\mathrm{He} + {}^{3}\mathrm{H} + 4.78\,\mathrm{MeV} \tag{3.1}$$

and ZnS(Ag) is the scintillation material. The two products of the reaction in Eq. (3.1), an α particle and a triton, interact with the ZnS inorganic scintillator grains mixed into the same matrix and a scintillation light (photons) is produced. The scintillation light is the result of the de-excitation of the luminescence centers in the ZnS molecules [25].

The generated photons travel through the single optical fiber which is coupled to a Photo-Multiplier (PM) tube (Hamamatsu R9880U-210) where the photons are converted into electrons, and where a D-type socket assembly (Hamamatsu E10679-02) acts as a voltage divider.

The neutron detection system including the scintillator, optical fiber and PM tube, needs to be connected to a Data Acquisition System (DAS). For the experiments conducted at Chalmers University of Technology, the signal coming from the PM tube is amplified and enhanced with an amplifier. The signal then goes through a discriminator, where it has to be higher than a certain threshold to be considered meaningful. The discriminator helps to reduce noise and parasitic signals. At the last stage, the output from the discriminator reaches an analog counter, which registers the neutron count rate with respect to the measurement time. For the experiments performed at SCK CEN the DAS consisted of a pre-amplifier and a Multi-channel Analyzer (MCA) connected to a digital software. The pre-amplifier integrates the incoming signal and the MCA sorts the pulses into a spectrum of number of events versus the pulse height. The spectrum is displayed on the software where discrimination can be applied by an offline threshold in addition to other data analysis processes.

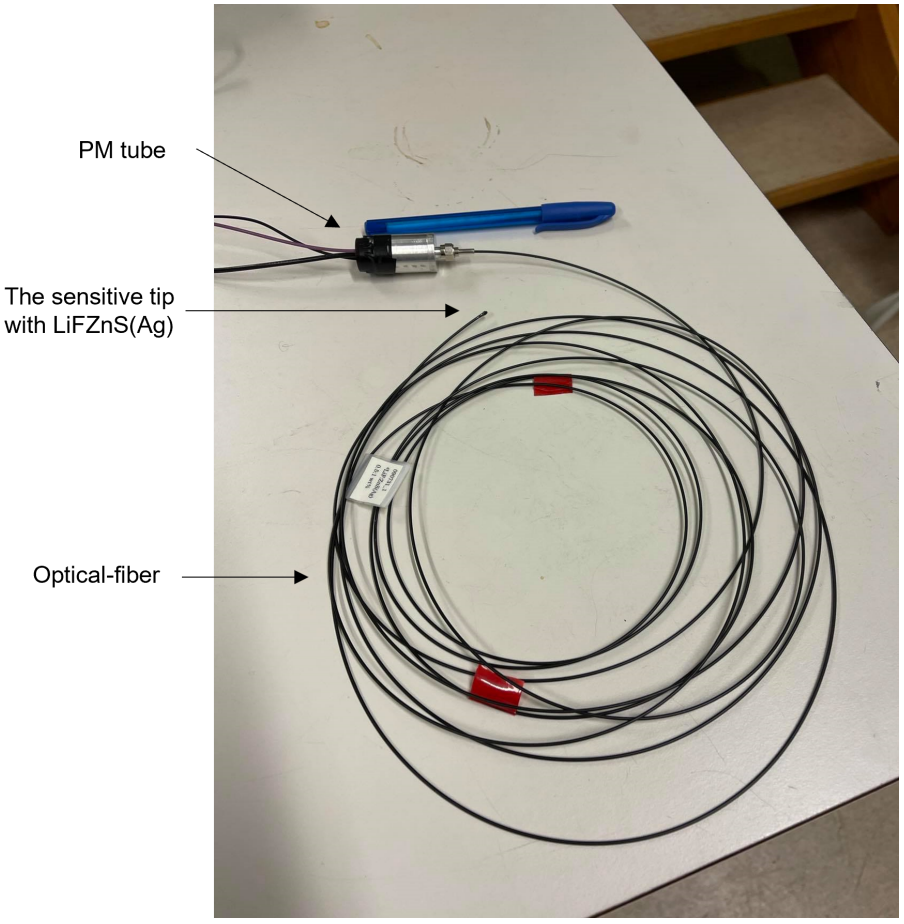

Figure 3.1: One of the two optical fiber-based scintillators.

3.2 Experiment in the hot-cell laboratory

The first set of experiments were performed in the hot-cell laboratory at the Department of Physics, Chalmers University of Technology. The sensitive parts of the scintillators are placed one at a time near an Americium-Beryllium (Am-Be) neutron source surrounded by polyethylene plates, see Figure 3.2. The Am-Be source has an activity of 5 curie and an emission rate of 1.1×10^7 n/s and is stored in a small steel canister (3 cm in radius and 6 cm in height) for a safe handling. The neutron source is surrounded by polyethylene plates from all sides to act as a moderator for slowing down the neutrons emitted from the source. The thermalisation of the neutrons emitted from the source is needed since the detectors are mainly sensitive to neutrons in the thermal energy range.

Ten measurements were performed with each scintillator, with a measurement time of 10 s each. The neutron counts were recorded from the counter after each measurement, and the histograms of the counts/10 s for the two scintillators (denoted as A and B) are shown in Figure 3.3. The mean value and the standard deviation of the neutron count rates are reported in Table 3.1. Scintillator A tends to provide a slightly higher neutron count rate as compared to scintillator B. These kind of deviations are expected, since the neutron-sensitive tips and the coupling between the optical fibers and the PM tubes were made by hand. Nevertheless, the two scintillators are proven to provide relatively close count rates for thermal neutrons.

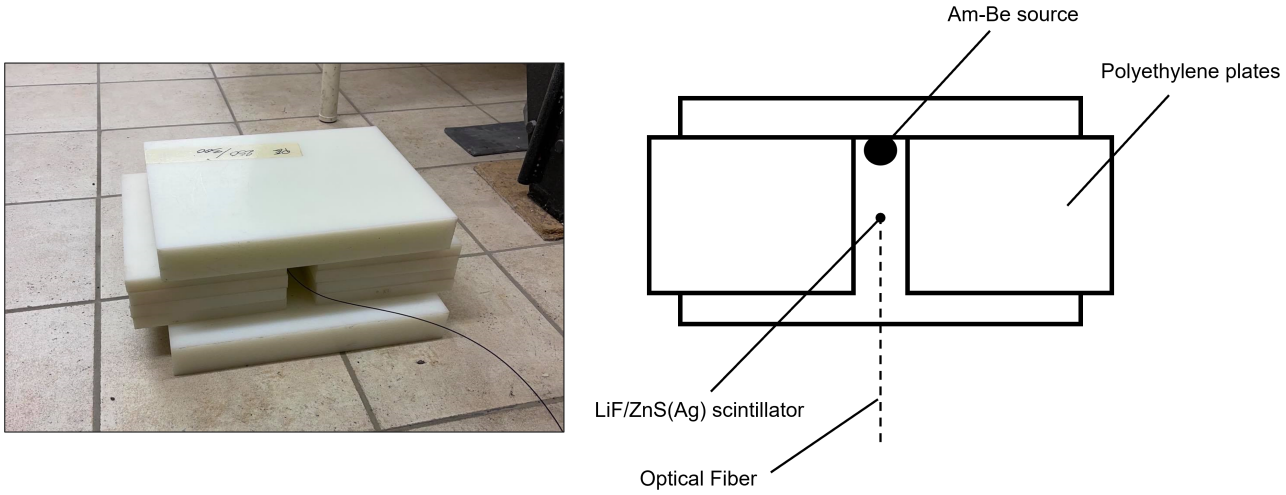

Figure 3.2: Set-up of the experiment in the hot-cell laboratory at Chalmers.

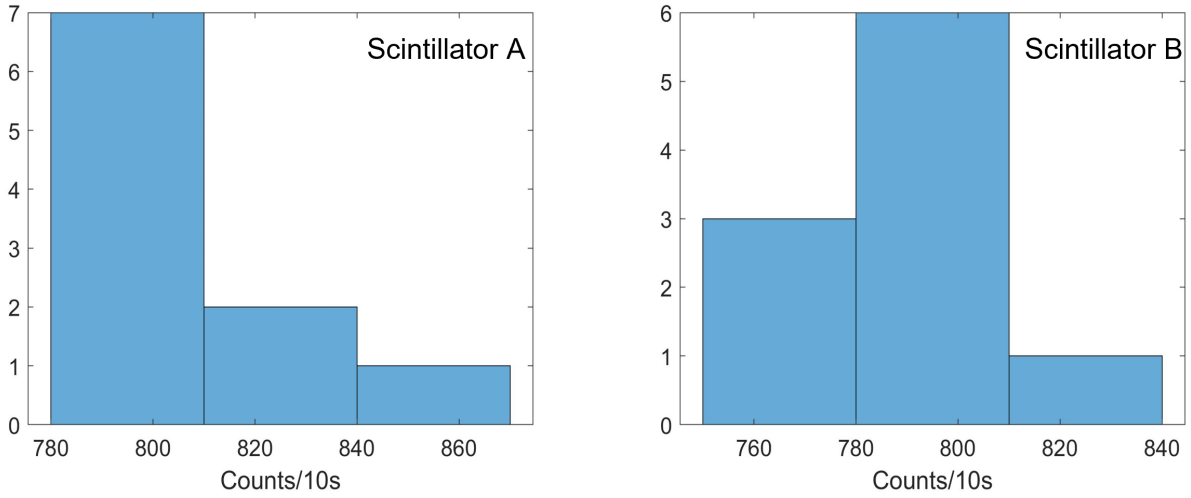

Figure 3.3: Neutron count rate from Scintillator A (left) and from Scintillator B (right).

Table 3.1: Mean value and standard deviation of the neutron count rates from the scintillators.

Scintillator	Count rate (/10 s)	
	Mean value	Standard deviation
A	808.5	18.5
B	791.3	16.8

3.3 Experiment in the BR1 research reactor at SCK CEN

Further characterization of the two scintillators was carried out in the BR1 research reactor at SCK CEN in order to determine the sensitivity to thermal neutrons, the calibration factors and the relative efficiencies.

The BR1 was the first research reactor in Belgium and was commissioned in 1956 [26]. The reactor is air-cooled and graphite-moderated, see its schematic view in Figure 3.4. At the top of the reactor a spherical cavity with a radius of 50 cm is available for irradiation experiments and calibration of detection instruments under a well-defined Maxwellian thermal neutron flux. The neutron flux at the center of the cavity is constantly monitored using a calibrated fission chamber.

The two scintillators were inserted into the cavity one at a time using customized aluminum rods as the one shown in Figure 3.5. The fibers were taped to the inside of the aluminum rods with their tips at the bottom of the rod. The rods were then inserted into the cavity from the top. When the rod is fully inserted, its bottom is located exactly at the centre of the cavity.

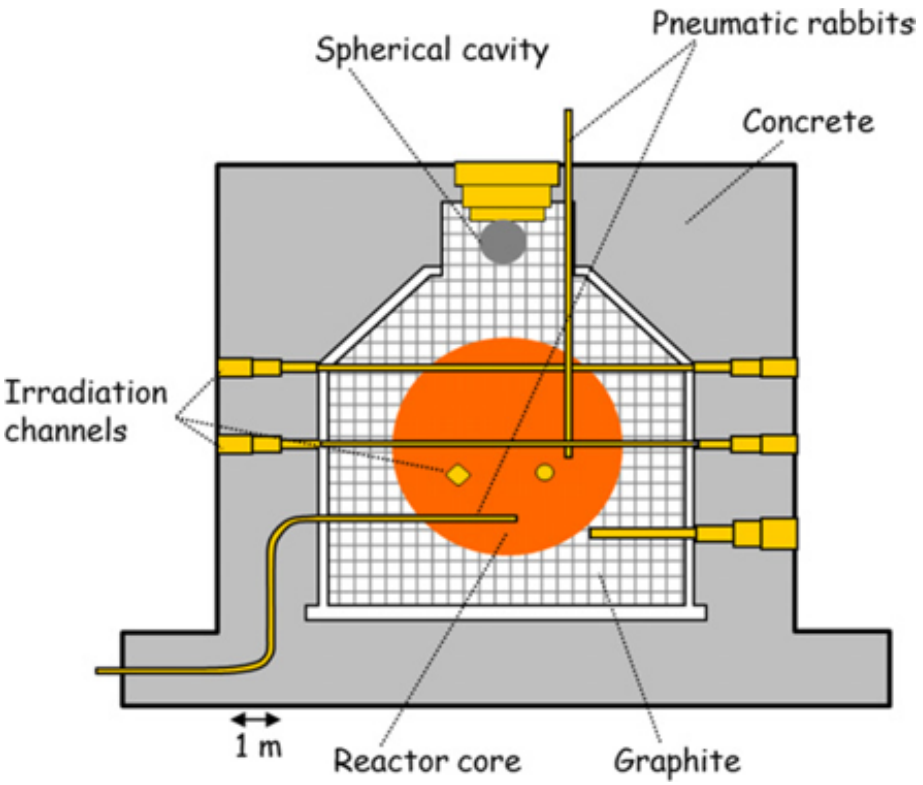

Figure 3.4: Schematic of the BR1 research reactor [26].

At first, background measurements were performed with both scintillators while inserted in the cavity with the reactor being turned-off. The background count rate was negligible for both scintillators. The reactor was then turned-on and the neutron count rate was recorded for each scintillator, at the centre of the cavity, at different reactor power levels. The measurements were performed after the reactor reached criticality at each power level and the measurement time was chosen to be 10 minutes each. Figure 3.6 shows how the neutron count rate from each scintillator increases with increasing the power level of the reactor. As already observed in the experiments

Figure 3.5: Aluminum rods used to insert the scintillators in the reactor cavity.

in the hot-cell laboratory at Chalmers University of Technology, scintillator A tends to provide higher neutron count rates compared to scintillator B.

The conventional thermal neutron flux in the center of the cavity can be obtained by multiplying the corrected count rate of the monitor fission chamber with a calibration factor (CF), i.e.:

$$CF = \frac{Conventional\ Thermal\ Neutron\ Flux\ (cm^{-2}s^{-1})}{Monitor\ Fission\ Chamber\ Count\ Rate\ (s^{-1})} = (2.60 \pm 0.03)10^4\ (cm^{-2}) \quad (3.2)$$

The count rates from the fission chamber and the correction factor were provided by the reactor operators and the values of the thermal neutron flux at each power level are listed in Table 3.2. The ratio between the count rate from the neutron scintillators and the conventional thermal flux at the center of the cavity represents the sensitivity of the scintillators in (cm^2):

$$Sensitivity_{A,B}\ (cm^2) = \frac{Count\ Rate\ From\ Det_{A,B}\ (s^{-1})}{Thermal\ Neutron\ Flux\ (cm^{-2}s^{-1})} \quad (3.3)$$

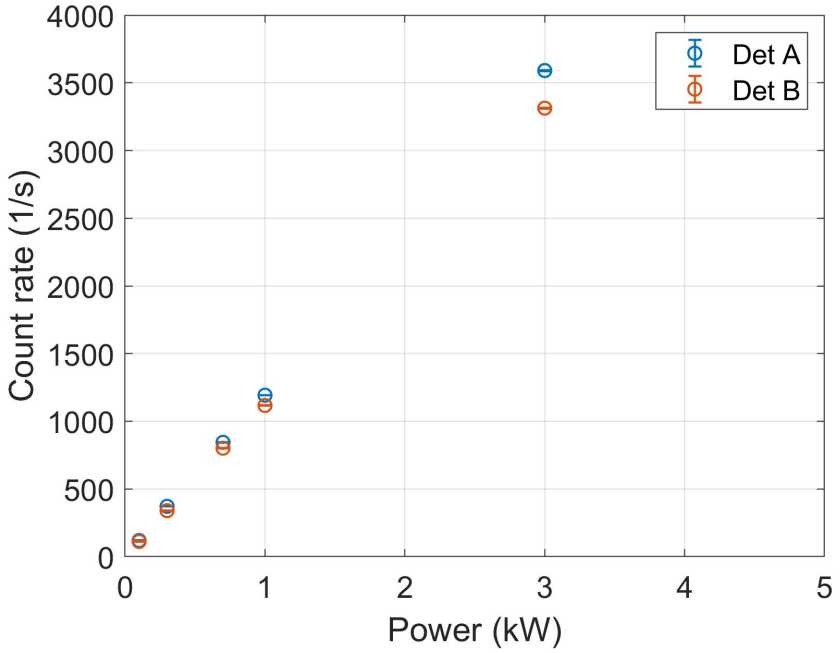

Figure 3.6: Neutron count rates from scintillators A and B with respect to the reactor power.

This ratio should be the same at all power levels, and Table 3.3 shows that this is indeed the case. Thus, the fiber-based neutron scintillators are proven to be viable for estimating accurately the thermal neutron flux. The sensitivities given in Table 3.3 can serve as a calibration factor, similar to the one from the calibrated fission chamber, so that the thermal neutron flux at one point can be obtained from the neutron count rate of the scintillators at the same point.

Table 3.2: Thermal flux at the center of the cavity, at different power levels.

Power (kW)	Flux ($cm^{-2}s^{-1}$)	Uncertainty ($\pm$)
0.1	$1.04E+05$	$1.92E+03$
0.3	$2.86E+05$	$4.80E+03$
0.7	$6.76E+05$	$9.48E+03$
1	$9.62E+05$	$1.28E+04$
3	$2.91E+06$	$3.88E+04$

Table 3.3: Sensitivities of scintillators A and B and their relative efficiencies at different power levels.

Power (kW)	Sensitivity A (cm^2)	Uncertainty (%)	Sensitivity B (cm^2)	Uncertainty (%)	Relative efficiency B/A (%)	Uncertainty (%)
0.1	$1.15E-03$	1.87	$1.08E-03$	1.86	93.82	2.48
0.3	$1.30E-03$	1.69	$1.19E-03$	1.69	91.43	2.19
0.7	$1.25E-03$	1.41	$1.19E-03$	1.40	94.88	1.89
1	$1.24E-03$	1.34	$1.16E-03$	1.34	93.63	1.77
3	$1.23E-03$	1.33	$1.14E-03$	1.34	92.26	1.74

The relative efficiency of scintillator B compared to that of scintillator A is calculated as:

$$Relative\ Efficiency_{B/A}\ (cm^2) = \frac{Sensitivity_B\ (cm^2)}{Sensitivity_A\ (cm^2)} \times 100\% \tag{3.4}$$

The values of the relative efficiency for all measurement points are included in Table 3.3 and are almost constant and thus independent from the power level. Consistently with the results in the experiment carried out at Chalmers University of Technology and with the count rates of Figure 3.6, the scintillator A has a higher efficiency.

The detector response to spatial variation of the neutron flux was also measured at different axial positions in the BR1 cavity. Figure 3.7 shows the comparison between the axial flux profiles (relative to the flux at the centre of the cavity) obtained from the scintillators A and B and a best-fitting of measurements from the calibrated fission chamber. The overall agreement is good, although discrepancies are found for positions between 30 cm and 40 cm from the center of the cavity.

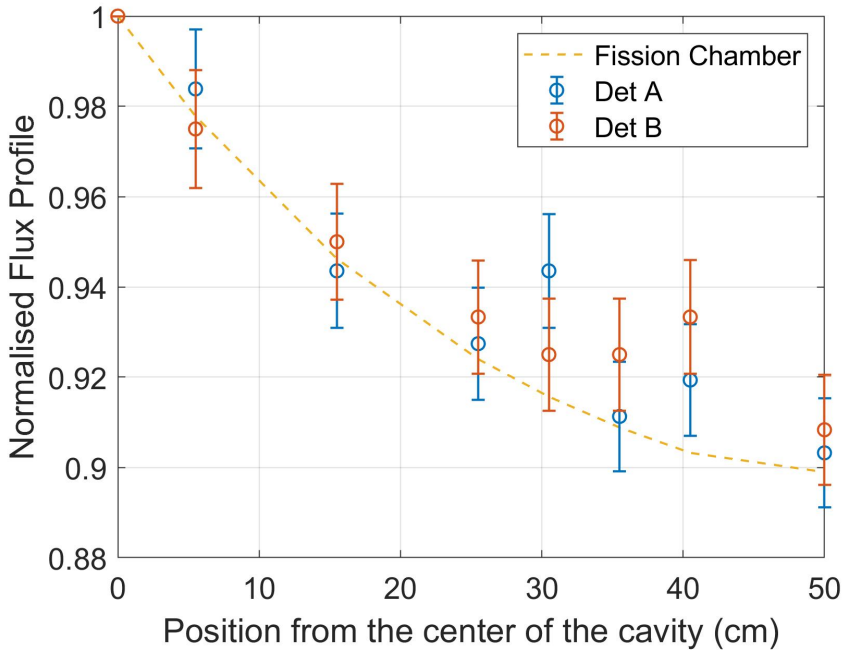

Figure 3.7: Axial neutron flux profile relative to the flux at the centre of the BR1 cavity; comparison between scintillators A and B and a best-fitting of measurements from the calibrated fission chamber.

3.4 Experiment in LNK at SCK CEN

In the context of the current project, the neutron scintillators are planned to be used within spent nuclear fuel assemblies. In such an environment, detectors are exposed to both a neutron flux and a gamma dose rate. Therefore, it is important to test the sensitivity of the scintillators, optical fibers and PM tubes to gamma rays as well. If the whole detection system is not properly shielded, gamma rays may cause undesired contributions in terms of photons and thus an inaccurate estimation of the neutron flux. If the sensitivity to gamma rays is correctly identified, the detector could be calibrated accordingly by setting a proper discrimination threshold to discard the contribution of the gamma rays in the recorded count rate. To investigate this aspect, a third set of experiments was performed in the Laboratory for Nuclear Calibrations (LNK) at SCK CEN. The LNK facility operates a state-of-the-art calibration building constructed in 2021 and equipped with modern irradiators, reference instruments and data acquisition software.

In the experiment in LNK, the two scintillators were exposed to Cs-137 and Co-60 sources with different dose rates that varied in a range between 5 mGy/h and 200 Gy/h. The scintillators did not show any response to gamma rays for dose rates below $\sim$ 70 Gy/h. For higher dose rates, the scintillators were placed at the closest distance to the collimator of a Co-60 source (77.19 Gy/h), as shown in the experimental setup in Figure 3.8. For a higher dose rate (approximately 200 Gy/h), the scintillators were placed inside the collimator. The count rates from both scintillators were affected at these two dose rates, see Figure 3.9. Again, scintillator A provides slightly higher results in comparison with scintillator B.

This experiment proves that the neutron scintillators do have a sensitivity to gamma radiation. In a spent fuel assembly the gamma dose rate can be up to 1000 Gy/h [27] which is much higher than 200 Gy/h, so further testing is required to study the behavior of the scintillators under gamma radiation.

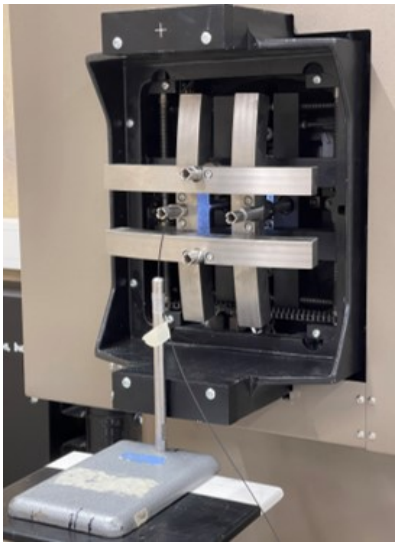

Figure 3.8: Set-up for the experiment with Co-60 at the LNK facility.

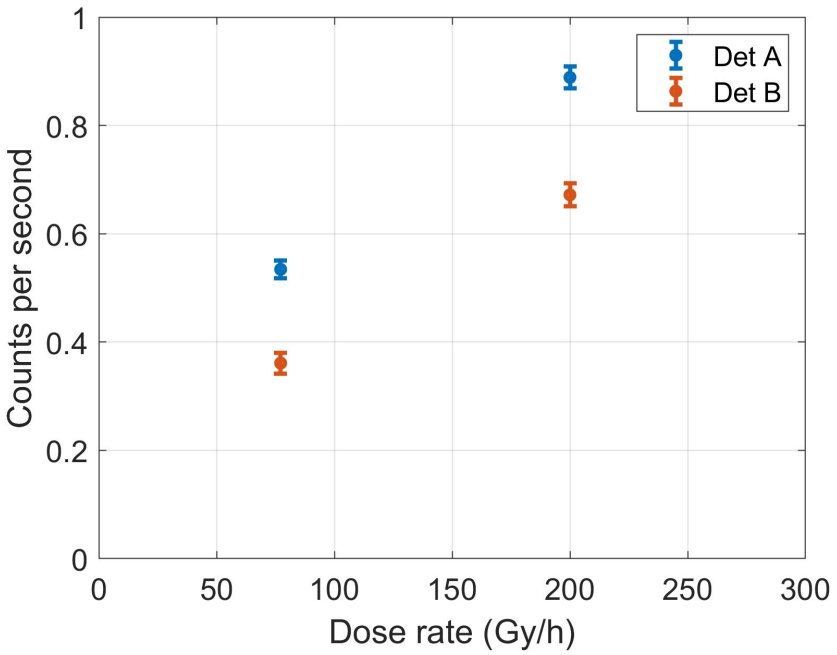

Figure 3.9: Count rates from scintillators A and B at different gamma dose rates.

4 Machine learning for inspection of spent nuclear fuel assemblies

The detector described in Chapter 2 and under development in the current project will allow to perform neutron flux and neutron flux gradient measurements inside spent nuclear fuel assemblies. Then this information can be used to discern if the assembly is intact or if fuel pins have been removed and/or replaced by dummy rods and from which position. The analysis of the neutron measurements from the spent nuclear fuel assembly to reconstruct the actual configuration of the system (and thus to find possible partial defects) is a typical inverse problem that can be efficiently solved with identification algorithms based on machine learning.

This chapter concerns the first step in the development of an identification algorithm for partial defects in spent nuclear fuel using an Artificial Neural Network (ANN). Basics of ANNs are introduced in section 4.1. The initial training and testing of the ANN model is carried out with only synthetic neutron flux measurements in PWR fuel assemblies, as discussed in sectio 4.2. The performance of the ANN algorithm is then compared with other machine learning algorithms, see section 4.3.

4.1 Basics of Artificial Neural Networks

Artificial Neural Networks (ANNs) are an advanced approach for machine learning and deep learning tasks. They can model non-linear relationships and thus learn and identify complex patterns through large datasets. Examples of their application can be found in systems for image, voice and text recognition [28]. ANNs are attractive for the investigation of partial defects in spent nuclear fuel assemblies because they may enable a more detailed evaluation of the system configuration which is needed, e.g., for a precise localization of the possible missing fuel pins.

Different architectures and strategies can be used to construct ANNs. In the current context, a typical feed-forward ANN [29] has been chosen and it consists of interconnected neurons, arranged in an input layer, one or more hidden layers, and an output layer, see Figure 4.1.

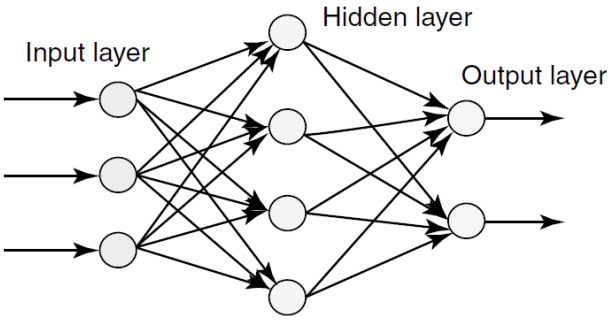

Figure 4.1: Generic schematic of a feed-forward artificial neural network [29].

To provide correct and usable predictions, a Neural Network needs to be trained, i.e., its model requires a proper tuning with the problem under study. Then sets of inputs and outputs that

represent true cases of the specific application of interest are used to make the neural network learn the relationship and the mapping between inputs and outputs.

The network receives a set of inputs (x_i, i=1...n) via the input layer. The input quantities take weights in the neurons, are combined according to the connections between the neurons and moved progressively through the hidden layers until they reach the output layers where the output result is delivered. The processing is regulated through hyper-parameters such as, the number of neurons and layers, the activation function, the optimizer function and the loss function.

The neurons are usually selected so that their number in the input layer is equal to the number of input features, and their number in the output layer is equal to the size of the output. For the hidden layers, the number of neurons needs to be tuned in order to optimize the performance of the algorithm.

The activation functions are mathematical gates in between the input feeding the current neuron and its output going to the next layer. Artificial neural networks use non-linear activation functions in order to learn more complicated patterns. The non-linearity also allows for back-propagation. This is a standard method to fine-tune the weights of the network in the training via the error rate obtained in the previous iteration [30]. Such a procedure makes the model more general and reliable. A neural network without an activation function is simply a linear regression model. Different activation functions can be chosen, depending on the problem to process. Some popular activation functions [31] are: the Sigmoid, the Hyperbolic Tangent (Tanh), the Rectified Linear Unit (ReLU) and the Softmax.

The optimizer is an algorithm that is used to change the attributes of the neural network such as the weights and the learning rates in order to reduce the losses (errors). Some popular optimization functions [32] are: the Gradient Descent, the Stochastic Gradient Descent, the Nestrov Accelerated Gradient, the Adaptive Gradient (AdaGrad) and the Adaptive Moment Estimation (AdaM).

A loss function is needed to estimate the error of the model during the optimization process. The loss function calculates how closely the distribution of the model predictions matches the distribution of the target variables in the training data. Some popular loss functions [33] are: the Logarithmic Loss (Cross-Entropy) and the Categorical Cross-Entropy.

The accuracy of an ANN model can be estimated via a N-fold cross-validation process. Accordingly, the whole dataset is shuffled and divided into N random batches. N-1 of these batches are used for the training, while the remaining one is used as a testing dataset. The process is repeated N times so that each of the N batches can serve as testing dataset. The final estimate of the model accuracy is taken as the average of the accuracy on the testing dataset calculated in the N repetitions. The result will then be less biased and the prediction capability of the model can be evaluated in a fairer manner when compared with other types of models. However, the cross-validation is computationally expensive since it requires the development of a separate model for each repetitions.

For the training of the ANN, the number of epochs and the batch-size are key-parameters to select. The batch-size represents the number of training samples that the ANN needs to process before updating its internal parameters. The number of epochs determines the number

of complete passes the network makes through the entire dataset. These parameters have no default/preferable values, therefore they have to be optimized with respect to the problem at-hand in order to avoid over- or under-fitting of data.

4.2 Development of an ANN algorithm for partial defects in spent nuclear fuel

One of the objectives of the current project is to develop an ANN algorithm that can process neutron flux and neutron flux gradient measurements from a spent nuclear fuel assembly and identify possible partial defects. As a starting point, a dataset based only on simulated neutron flux measurements in PWR fuel assemblies (section 4.2.1) is used to train and test the ANN algorithm (section 4.2.2). The extension of the dataset to neutron flux gradient is planned at a later stage of the project.

4.2.1 Available dataset

The database for an initial training and testing of the ANN algorithm relies on previous work performed at SCK CEN [20, 21]. The overall set consists of synthetic data generated via Monte Carlo simulations of the response of specific detection techniques for intact 17x17 PWR spent nuclear fuel assemblies and a variety of hypothetical diversion scenarios in which different number of fuel pins have been replaced by dummy pins made of stainless steel. The detection techniques that are included in the previous work [20, 21] are non-destructive assay (NDA) techniques, e.g., the fork detector and the Partial Defect Tester (PDET). At this stage of the project, only the part of the dataset for PDET is used because the neutron flux is evaluated in the guide tubes of the fuel assemblies, which is similar to the strategy followed in the application of the gradient detector described in Chapter 2.

The PDET consists of a set of neutron and gamma-ray detectors that are positioned inside the empty guide tubes of a PWR fuel assembly and outside the assembly in order to measure the passive emission of neutrons and gamma-rays from spent fuel [34, 35]. The first prototype of the PDET instrument was developed by Lawrence Livermore National Laboratory (LLNL) [36] and then further developed by SCK CEN [21].

The database contains 1160 different full assembly models; 197 cases of intact assemblies with varying Initial Enrichment (IE, between 2 and 5w%), Cooling Time (CT, 1 to 50 years) and Burn-Up (BU, 5 to 60 MWd/kgU) and 963 cases of both symmetric and asymmetric diversion scenarios, as shown in Figure 4.2, with varying IE and BU. The results of the Monte Carlo simulations (e.g., the neutron flux in the guide tubes of the assemblies) are the input features of the machine learning model, and the class label based on the percentage of replaced fuel pins represents the model response (output). Seven class labels were defined for the response, representing complete fuel assemblies (class 0) and fuel assemblies with increasing number of replaced pins (classes 1 to 6 as reported in Table 4.1). Then, the problem corresponds to a supervised, multi-class classification problem.

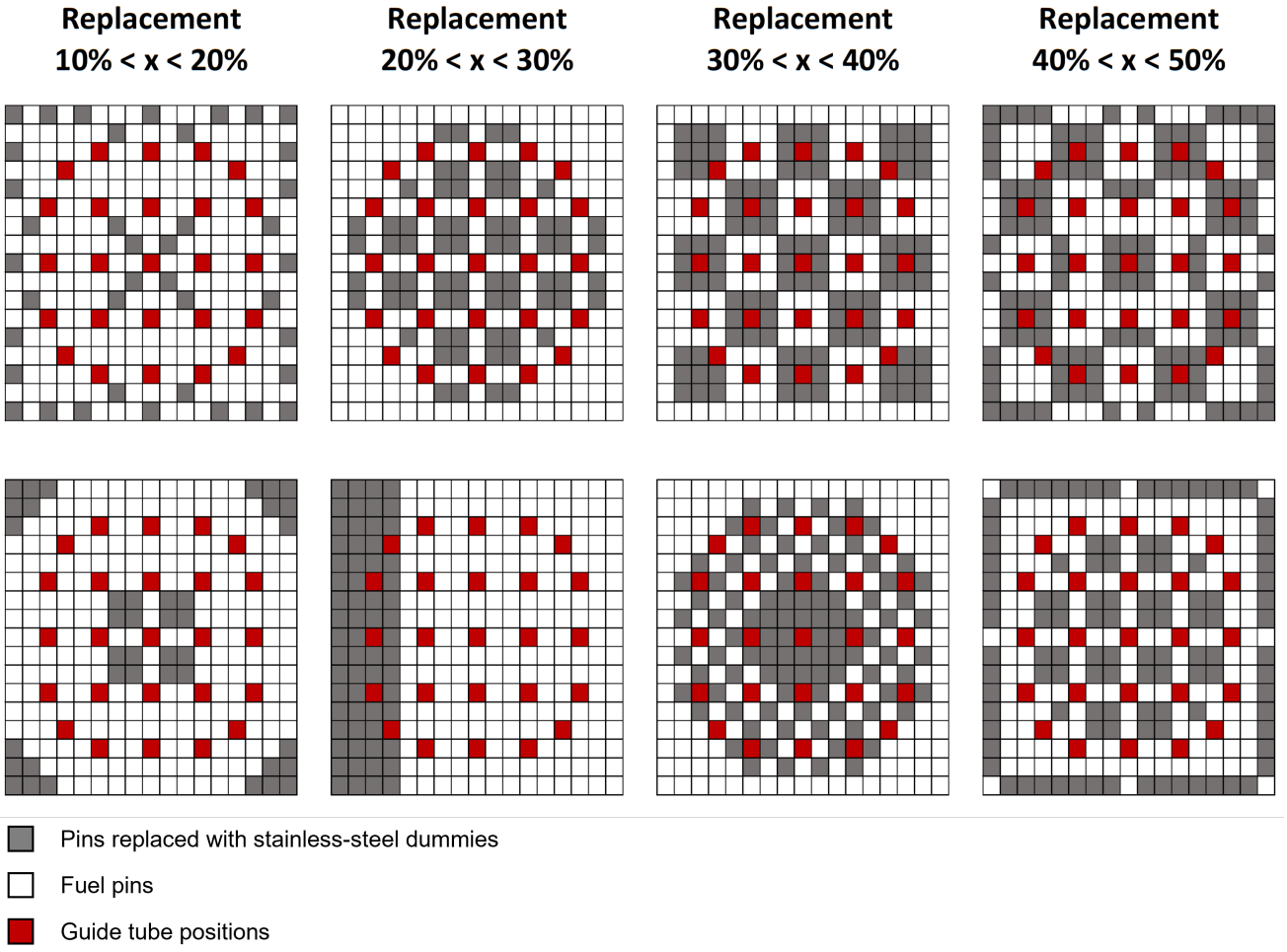

Figure 4.2: Examples of diversion scenarios included in the dataset [21].

Table 4.1: Class labels with respect to the percentage of replaced fuel pins.

Percentage of replaced pins	Class label	Number of observations
0	0	196
$<= 10\%$	1	171
$10\% < x < 20\%$	2	216
$20\% < x < 30\%$	3	189
$30\% < x < 40\%$	4	144
$40\% < x < 50\%$	5	144
$>= 50\%$	6	99

4.2.2 Settings and Training

A sequential neural network model with 1 hidden layer was built using the TensorFlow [37] and the Keras [38] open-source software libraries.

The Rectified Linear Unit (ReLU) activation function is used in the input layer and in the hidden layer because of its computational efficiency and quick convergence rate. The SoftMax activation function is used in the output layer because it can provide, in a multi-class problem, the probability of an input value to be in a specific class.

The Adaptive Moment Estimation (ADAM) optimizer was chosen as optimizer because it can converge at a fast rate and overcome vanishing learning rates and high variances.

The evaluation of the error (loss) of the algorithm in the optimization process is obtained from the Categorical Cross-Entropy loss function, which can handle multiple classes.

For the training, different numbers of epochs and different batch-size are tested simultaneously. Figure 4.3 shows how the classification accuracy on the training dataset changes with changing the number of epochs (from 1 to 3000) and the batch-size (from 5 to 100). Based on these results, a number of epochs of 1000 and a batch-size of 5 are selected.

The number of neurons in the hidden layer is varied from 0 to 192 and the results are shown in Figure 4.4. Then a number of neurons of 96 is considered to be optimal for the current application.

4.3 ANN compared with Decision Trees and k Nearest Neighbors

The ANN model discussed in section 4.2 is compared with two different non-parametric supervised learning methods, namely the decision tree (DT) and the k-nearest neighbors (kNN). For this purpose, the DT and kNN models for safeguards applications developed at SCK CEN were used [20].

4.3.1 Decision Tree algorithm

Decision trees are one of the most commonly used and easy to implement models of machine learning. The decision tree algorithm developed at SCK CEN relies on binary trees, i.e., the internal nodes contain only one incoming branch and two outgoing branches. According to a splitting criterion based on the value of one input feature, each internal node in the decision tree

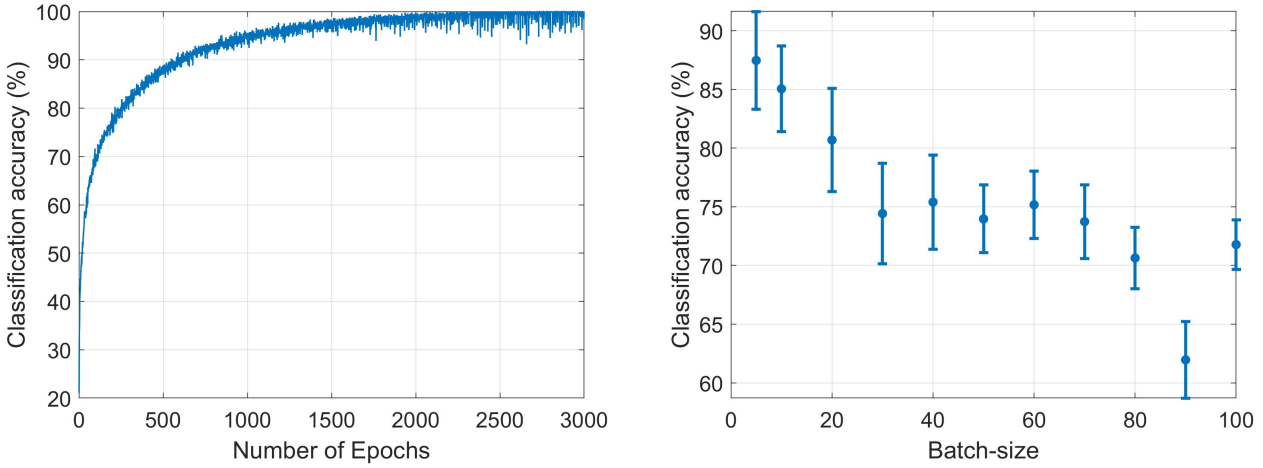

Figure 4.3: Classification accuracy of the ANN with 96 neurons in the hidden layer with: varying number of epochs (batch size=5) (left), and varying batch size (of epochs=1000) (right).

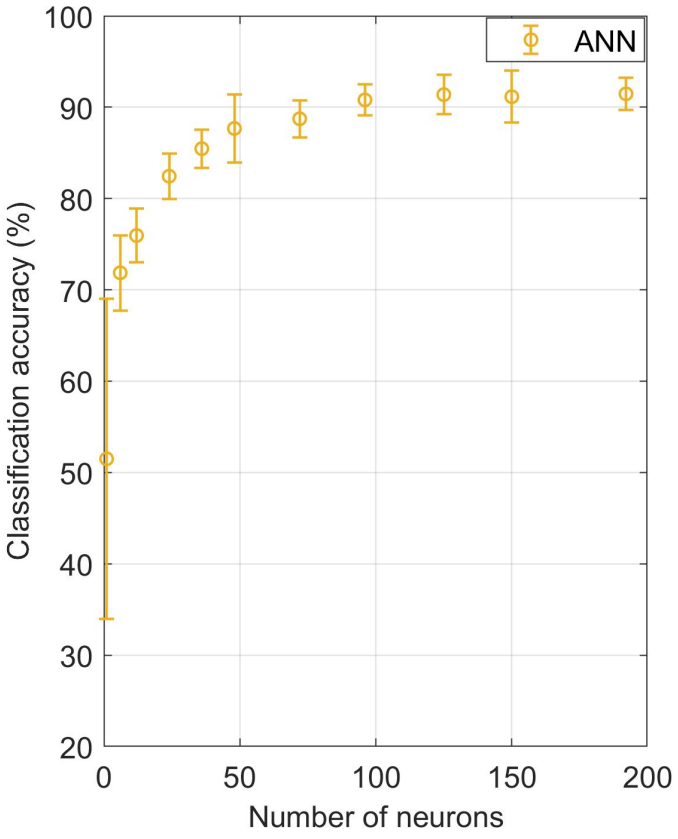

Figure 4.4: Classification accuracy of the ANN with respect to the number of neurons in the hidden layer.

splits the observations into two groups. At the end, each leaf node is assigned to one class label which is the class label of the majority of the training observations that reach the leaf node.

Given the simulated neutron flux measurements from the database described in section 4.2.1, the hyper-parameters of the decision tree are tuned-in. The maximum number of splits (tree depth) is varied from 2 to 25, the minimum number of observations in one branch is kept to the default value which is 10. The minimum number of observations in one leaf node is also kept to the default value, i.e. 1. The Gini diversity index [39] (Gini impurity) is chosen as the splitting criterion.

The classification accuracy is estimated via a cross-validation process which is similar to the one described in section 4.1 for ANNs and makes use of 5 random batches.

The evaluation of the classification accuracy shows that a higher tree depth, within the range between 1 and ~ 15, leads to a better performance, see Figure 4.5. To avoid overfitting of the training dataset, a tree depth of 10 can be considered optimal.

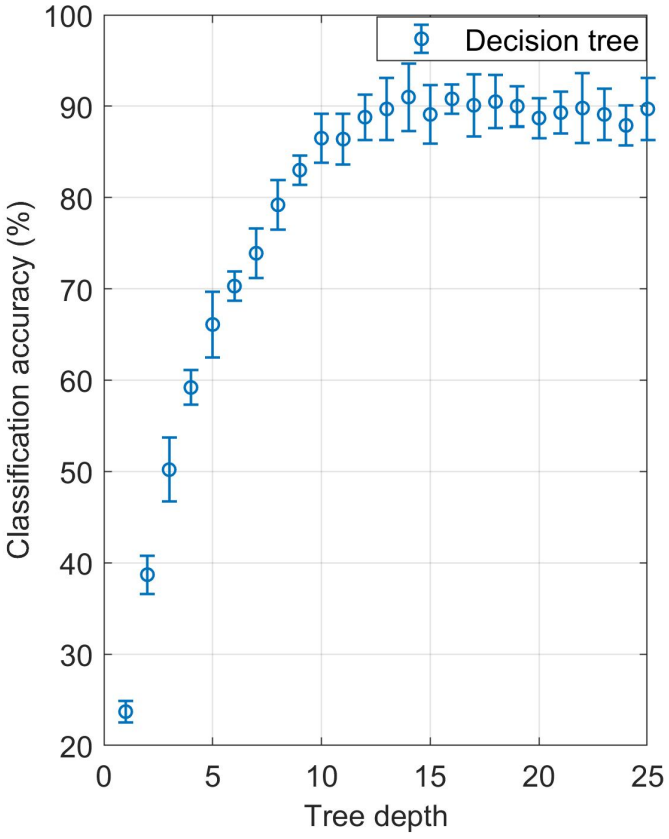

Figure 4.5: Classification accuracy of the DT algorithm.

4.3.2 k Nearest Neighbors

The k nearest neighbors (kNN) model is used to classify the observations into separate classes based on the distance from k neighboring observations. The most important steps in building the kNN model are: the selection of the input features used in the model, the approach used to calculate the distance between the observations, and the choice of the number of neighbors (k) that are considered for the classification.

The hyper-parameters of the kNN model are tuned-in for the dataset discussed in section 4.2.1. The Euclidean distance metric [40] is applied and equal weight is assigned to all training observations.

Similar to the case of the DT algorithm, the classification accuracy is estimated via a 5-fold cross-validation process. The variation of the classification accuracy with respect to the k number, varying between 1 and 25, is shown in Figure 4.6. Higher k-values lead to lower accuracy and a k-value of 5 can be optimal to not over-fit the training dataset.

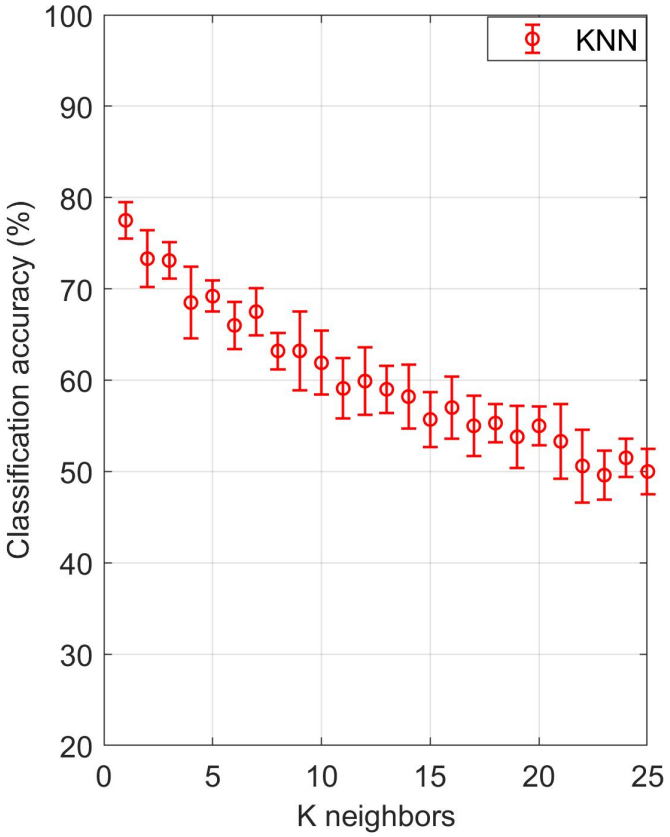

Figure 4.6: Classification accuracy of the kNN algorithm.

4.3.3 Comparison

The ANN, DT and kNN algorithms are compared via Figures 4.4, 4.5 and 4.6. For an optimal choice of the parameters, the ANN (with 96 neurons) and DT (with tree depth equal to 10) have a similar classification accuracy (90.8% for the ANN and 86.5% for the DT), while the kNN (with a number of neighbors of 5) has a worse performance, the classification accuracy being equal to 69.2%.

More insights can be obtained from the confusion matrix of each algorithm, see Figure 4.7. The confusion matrix provides a summary of the number of correct and incorrect predictions of one algorithm, for each class included in the database. The different number of cases per class label

in the case of ANN, compared to DT and kNN, is due to the random shuffling of the dataset prior to the splitting into the training and testing subsets.

The results show that the majority of the misclassifications from all three models appear in classes 1 to 3 (assemblies with 10-30% replaced fuel pins).

The most undesirable misclassification in terms of safeguards is a false negative, i.e., when a non-intact assembly is predicted as intact (class 0), since removed fuel will be undetected. The ANN model shows the best performance in terms of classification accuracy. However, the DT model gives the lowest number of false negatives.

For the current problem, the decision tree algorithm, even though its implementation is simple, has performances that are comparable to the performances of the artificial neural network. The use of a more complex approach such as artificial neural networks is expected to be more advantageous when more difficult problems are considered, such as the identification of the number and location of missing fuel pins from the measurements of the gradient detector.

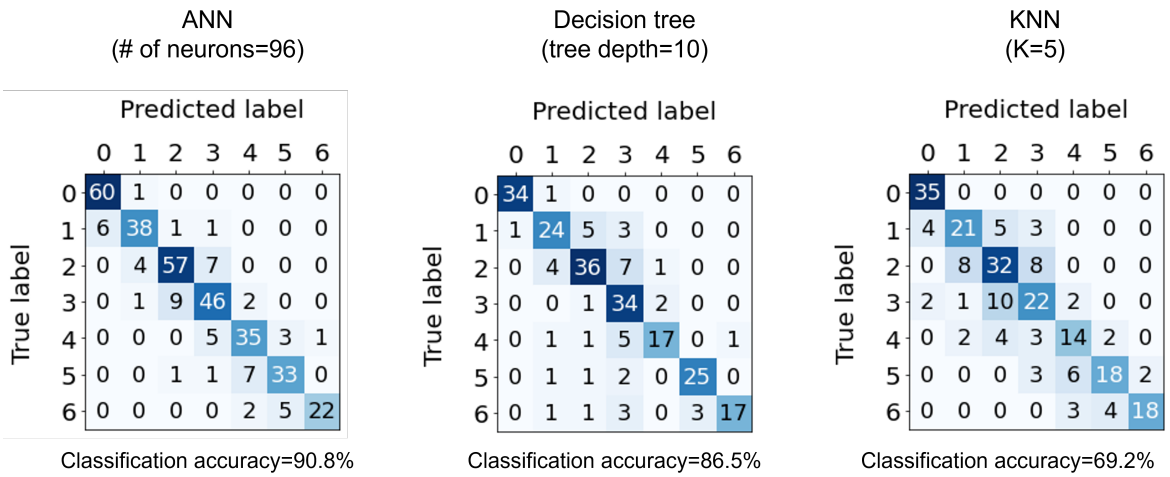

Figure 4.7: Confusion matrices for ANN, DT and kNN models applied to the PDET dataset.

5 Conclusions and future work

Conclusions and future work are discussed in section 5.1 and 5.2, respectively.

5.1 Conclusions

In this thesis different aspects have been explored for the development of a novel methodology for non-intrusive inspection of spent nuclear fuel. The methodology is based on two main steps: 1) measurements of the neutron flux and its gradient are performed in spent nuclear fuel assemblies using small neutron detectors; and 2) the measurements are processed using an ANN algorithm to identify number and location of possible fuel pins that have been removed from the fuel assemblies and replaced with dummies. The use of small neutron detectors simplifies the inspection procedure since the fuel assemblies do not need to be moved from their storage position. In addition, the neutron flux gradient measurements and its processing with the ANN algorithm may lead to more accurate results.

For the first step of the methodology, a new neutron detector that can measure the neutron flux gradient within a fuel assembly needs to be constructed. The design of the neutron gradient detector consists of four thin LiF-ZnS(Ag) optical fiber-mounted neutron scintillators arranged in an aluminium matrix in a rectangular pattern. Monte Carlo simulations were used to study the concept (Chapter 2, Paper I, and Paper II), and experiments were carried out to test and characterize two LiF-ZnS(Ag) optical fiber-based neutron scintillators (Chapter 3).

The outcome of the computational study of the gradient detector shows that the selected design is a viable option in terms of size and performance. The detector is small enough to be inserted in the guide tubes of PWR fuel assemblies, and the magnitude and direction of the neutron gradient vector in a neutron multiplying system, under different conditions, have been correctly retrieved from the reaction rates estimated via Monte Carlo calculations.

In the experimental work, two LiF-ZnS(Ag) optical fiber-based neutron scintillators (courtesy of KURNS, Japan) have been tested with a neutron source in the hot-cell laboratory at Chalmers University of Technology and in the BR1 research reactor at the Belgian Nuclear Research Centre (SCK CEN), so that their sensitivities to thermal neutron and relative efficiencies have been determined. Their sensitivity to gamma radiation has been also investigated in LNK (SCK CEN).

For the second step of the methodology, a machine learning algorithm based on an ANN is under development (Chapter 4). At this initial stage, a simpler problem has been considered, i.e., the ANN has been prepared, trained and tested using a dataset of synthetic neutron flux measurements that allow to classify PWR spent nuclear fuel assemblies according to the number of removed fuel pins. Such an ANN algorithm has been compared with a DT and a kNN algorithm. In the multi-class problem analyzed in this thesis, the ANN algorithm provide somewhat better results, although its implementation is much more complex than the one needed for DT and kNN methods. However, the ANN algorithm is expected to be more advantageous when processing richer inputs (e.g., the neutron flux and the neutron flux gradient measurements) and aiming at more detailed predictions (e.g., the identification of the number and location of the missing fuel pins in a fuel assembly).

5.2 Future work

In the continuation of this research, several developments are planned as follows:

- Monte Carlo simulations will be used to study the performance of the new detector in estimating the gradient of the neutron flux in PWR and BWR spent nuclear fuel assemblies. The intact configurations and examples of partial defects with different numbers of removed fuel pins and at different locations will be considered.
- Further experiments will be carried out to evaluate the sensitivity of the optical fiber-based neutron scintillators to gamma radiation fields that are typical of spent nuclear fuel assemblies.
- The gradient detector will be constructed and investigated for neutron gradient measurements in a MOX fuel assembly available at SCK CEN.
- A database that includes simulated neutron flux gradient measurements in fuel assemblies, with and without partial defects, will be generated and used for the training and testing of the ANN algorithm.
- The overall methodology that combines measurements with the neutron flux gradient detector and the processing of the measurements with the ANN algorithm will be verified.

References

[1] *World Nuclear Performance Report 2021, Report No. 2021/003, World Nuclear Association, England and Wales.* September, 2021.

[2] *Foundation Module, 1st ed, World Institute of Nuclear Security, Vienna, Austria.* 2016.

[3] H. Lee and M.-S. Yim, "Investigation of a fast partial defect detection method for safeguarding PWR spent fuel assemblies," *Annals of Nuclear Energy*, vol. 144, p. 107496, 2020.

[4] *IAEA Annual Report 2013, Report GC(58)/3, International Atomic Energy Agency, Vienna, Austria.* 2014.

[5] Stephen J. Tobin and Peter Jansson, *Nondestructive assay options for spent fuel encapsulation, Technical Report TR-13-30, Svensk Kärnbränslehantering AB, Swedish Nuclear Fuel and Waste Management Co, Stockholm, Sweden.* March, 2013.

[6] S. Jacobsson Svärd, A. Håkansson, A. Bäcklin, P. Jansson, O. Osifo, and C. Willman, "Tomography for partial-defect verification: experiences from measurements using different devices," *Esarda Bulletin*, vol. 33, pp. 15–25, 2006.

[7] K. van der Meer and M. Coeck, "Is the FORK detector a partial defect tester?," in *Safeguards Symposium*, IAEA, 2006.

[8] C. Mori, T. Osada, K. Yanagida, T. Aoyama, A. Uritani, H. Miyahara, Y. Yamane, K. Kobayashi, C. Ichihara, and S. Shiroya, "Simple and Quick Measurement of Neutron Flux Distribution by Using an Optical Fiber with Scintillator," *Journal of Nuclear Science and Technology*, vol. 31, no. 3, pp. 248–249, 1994.

[9] T. Yagi, H. Unesaki, T. Misawa, C. H. Pyeon, S. Shiroya, T. Matsumoto, and H. Harano, "Development of a small scintillation detector with an optical fiber for fast neutrons," *Applied Radiation and Isotopes*, vol. 69, no. 2, pp. 539–544, 2011.

[10] K. Watanabe, M. Yamanaka, T. Endo, and C. H. Pyeon, "Real-time subcriticality monitoring system based on a highly sensitive optical fiber detector in an accelerator-driven system at the Kyoto University Critical Assembly," *Journal of Nuclear Science and Technology*, vol. 57, no. 2, pp. 136–144, 2020.

[11] F. Vitullo, V. Lamirand, J.-B. Mosset, P. Frajtag, O. Pakari, G. Perret, and A. Pautz, "A mm^3 fiber-coupled scintillator for in-core thermal neutron detection in crocus," *IEEE Transactions on Nuclear Science*, vol. 67, no. 4, pp. 625–635, 2020.

[12] E. L. Brunetto, F. Vitullo, V. Lamirand, K. Ambrozic, D. Godat, M. Buck, G. Pohlner, J. Starflinger, and A. Pautz, "High resolution measurements with miniature neutron scintillators in the SUR-100 zero power reactor," *EPJ Web Conf.*, vol. 253, p. 04029, 2021.

[13] I. Pázsit and M. Kitamura, *Advances in Nuclear Science and Technology*, book section The Role of Neural Networks in Reactor Diagnostics and Control, pp. 95–130. Boston, MA: Springer US, 1996.

[14] I. Pázsit, N. S. Garis, and O. Glöckler, "On the Neutron Noise Diagnostics of Pressurized Water Reactor Control Rod Vibrations —IV: Application of Neural Networks," *Nuclear Science and Engineering*, vol. 124, no. 1, pp. 167–177, 1996.

[15] A. M. Durrant, G. Leontidis, S. Kollias, A. Torres, C. Montalvo, A. Mylonakis, C. Demaziere, and P. Vinai, "Detection and localisation of multiple in-core perturbations with neutron noise-based self-supervised domain adaptation," *Proc. Int. Conf. MC 2021, American Nuclear Society*, 2021.

[16] T. Tasakos, G. Ioannou, V. Verma, G. Alexandridis, A. Dokhane, and A. Stafylopatis, "Deep learning-based anomaly detection in nuclear reactor cores," in *Proceedings of the International Conference on Mathematics and Computational Methods Applied to Nuclear Science and Engineering (M&C 2021)*, October,2021.

[17] V. Mishra, E. Branger, Zs. Elter, S. Grape, and P. Jansson, "Comparison of supervised machine learning algorithms to predict PWR spent fuel parameters," in *INMM/ESARDA Joint Annual Meeting 2021*, 2021.

[18] M. Durbin and A. Lintereur, "Implementation of machine learning algorithms for detecting missing radioactive material," *Journal of Radioanalytical and Nuclear Chemistry*, vol. 324, no. 3, pp. 1455–1461, 2020.

[19] N. Shoman and B. B. Cipiti, "Unsupervised machine learning for nuclear safeguards.," tech. rep., Sandia National Lab.(SNL-NM), Albuquerque, NM (United States), 2018.

[20] R. Rossa, A. Borella, and N. Giani, "Comparison of machine learning models for the detection of partial defects in spent nuclear fuel," *Annals of Nuclear Energy*, vol. 147, p. 107680, 2020.

[21] R. Rossa, A. Borella, and K. van der Meer, "Comparison of the SINRD and PDET detectors for the detection of fuel pins diversion in PWR fuel assemblies," in *Proc. INMM-59 Annual Meeting*, 1 October 2018.

[22] J. Leppänen, "The Serpent Monte Carlo code: Status, development and applications in 2013," *Annals of Nuclear Energy*, vol. 82, pp. 142–150, 12015.

[23] P. Lindén, J. K. H. Karlsson, B. Dahl, I. Pázsit, and G. Por, "Localisation of a neutron source using measurements and calculation of the neutron flux and its gradient," *Nucl. Instr. Meth.*, vol. A 438, no. 2-3, pp. 345–355, 1999.

[24] S. Avdic, P. Lindén, and I. Pázsit, "Measurement of the neutron current and its use for the localisation of a neutron source," *Nucl. Instr. Meth.*, vol. A 457, no. 3, pp. 607–616, 2001.

[25] G. F. Knoll, *Radiation detection and measurement*. John Wiley & Sons, 2010.

[26] J. Wagemans, G. Vittiglio, E. Malambu, and H. A. Abderrahim, "The BR1 reactor: a versatile irradiation facility for fundamental research and industrial applications," in *The 1st International Conference on Advancements in Nuclear Instrumentation, Measurement Methods and their Applications, Marseilles, France*, June, 2009.

[27] T. Natsume, H. Doi, F. Ruddy, J. Seidel, and A. Dulloo, "Spent fuel monitoring with silicon carbide semiconductor neutron/gamma detectors," in *Reactor Dosimetry: 12th International Symposium*, ASTM International, 2007.

[28] A. K. Jain, J. Mao, and K. M. Mohiuddin, "Artificial neural networks: A tutorial," *Computer*, vol. 29, no. 3, pp. 31–44, 1996.

[29] A. Abraham, "Artificial neural networks," *Handbook of measuring system design*, 2005.

[30] J. Li, J.-h. Cheng, J.-y. Shi, and F. Huang, "Brief introduction of back propagation (bp) neural network algorithm and its improvement," in *Advances in computer science and information engineering*, pp. 553–558, Springer, 2012.

[31] S. Sharma, S. Sharma, and A. Athaiya, "Activation functions in neural networks," *towards data science*, vol. 6, no. 12, pp. 310–316, 2017.

[32] S. Vani and T. M. Rao, "An experimental approach towards the performance assessment of various optimizers on convolutional neural network," in *2019 3rd international conference on trends in electronics and informatics (ICOEI), Tirunelveli, India*, IEEE, April, 2019.

[33] K. Janocha and W. M. Czarnecki, "On loss functions for deep neural networks in classification," *arXiv preprint arXiv:1702.05659*, 2017.

[34] S. Sitaraman and Y. Ham, "Characterization of a safeguards verification methodology to detect pin diversion from pressurized water reactor (PWR) spent fuel assemblies using Monte Carlo techniques," in *Proceedings of the INMM 48th Annual Meeting, Tucson, AZ*, 2007.

[35] Y. S. Ham and S. Sitaraman, "Partial defect tester: A novel approach to detect partial defects in pressurized water reactor spent fuel," *Nuclear Technology*, vol. 175, no. 2, pp. 401–418, 2011.

[36] Y. Ham, P. Kerr, S. Sitaraman, R. Swan, R. Rossa, and H. Liljenfeldt, "Partial defect verification of spent fuel assemblies by PDET: Principle and field testing in interim spent fuel storage facility (CLAB) in Sweden," in *2015 4th International Conference on Advancements in Nuclear Instrumentation Measurement Methods and their Applications (ANIMMA)*, pp. 1–7, IEEE, 2015.

[37] M. Abadi *et al.*, "TensorFlow: Large-scale machine learning on heterogeneous systems," 2015. Software available from tensorflow.org.

[38] F. Chollet *et al.*, "Keras." https://keras.io, 2015.

[39] C. Caso and M. A. Gil, "The Gini-Simpson index of diversity: estimation in the stratified sampling," *Communications in Statistics - Theory and Methods*, vol. 17, no. 9, pp. 2981–2995, 1988.

[40] N. Bouhmala, "How good is the Euclidean distance metric for the clustering problem," in *2016 5th IIAI International Congress on Advanced Applied Informatics (IIAI-AAI)*, pp. 312–315, 2016.